2013

Beam Deflection

Matthias Münnich,
University of Central Florida

BEAM DEFLECTION

by

MATTHIAS MÜNNICH
B.S. Friedrich Schiller Universität , 2011

A thesis submitted in partial fulfilment of the requirements
for the degree of Master of Science
in the Department of Physics-Photonics
in the College of CREOL
at the University of Central Florida
Orlando, Florida

Summer Term
2013

ABSTRACT

In order to fully understand the third order nonlinear optical response of materials under high irradiance excitation it is necessary to study the temporal and polarization dependence of nonlinear refraction and absorption. There are several existing approaches such as Z-scan and pump-probe techniques to determine those responses. As part of this work, these approaches will be briefly outlined before presenting beam deflection, applied from photothermal beam deflection, as an alternative experimental technique to determine the nonlinear refraction with its temporal and polarization dynamics. This technique measures the angle of the probe beam deflected via the index gradient of the material induced by strong excitation beam, to determine both the sign and magnitude of the nonlinear refraction. The temporal and tensor properties of the nonlinear refractive index can be determined by introducing a delay line, and by varying the polarization of the excitation and probe beam, respectively.

To demonstrate the practicality of the beam deflection technique, we performed measurements on Fused Silica, Carbon Disulfide and Zinc Oxide. Each of these samples shows quite different nonlinear responses. Amorphous fused silica exhibits nonlinear refraction purely from instantaneous electronic contribution; while Carbon Disulfide shows a much slower response, originating not only from the electronic contribution but also from non-instantaneous nuclear movements (e.g. molecular orientation). These two contributions can be separated by varying the polarization direction of the excitation and probe beam. By introducing lock-in detection technique, a sensitivity of $\lambda/5500$ can be achieved. In Zinc Oxide, a wide-bandgap semiconductor, we measure both nonlinear refraction and two-photon absorption simultaneously. Therefore the beam deflection is a sensitive technique, which can be used to measure the time and polarization dynamics of the nonlinear response of the material.

ACKNOWLEDGMENTS

I would first like to thank my professors Dr. Eric Van Stryland and Dr. David Hagan for giving me the opportunity to work with them and their group. I would like to thank the NLO group in no particular order, Honghua Hu, Matt Reichert, Trenton Ensley, Davorin Peceli and Manny Ferdinandus, Himansu Pattanaik, Brendan Turnbull and Peng Zhao for being great colleagues and all the help provided. In particular I would like to thank Manny Ferdinandus for introducing me to the lab and the experimental work and Honghua Hu for keeping me on track with the tight schedule. Moreover, I would like to thank the staff and supporters of the MILMI program that made it possible for me to participate in the MS program at CREOL and enabled me to pursue my degree. I would also like to thank my other American friends, all the Triknights and the MILMI students that shared with me the amazing time. Lastly, and perhaps most importantly I would like to thank my family. My parents for the constant encouragement and for doing everything possible to help and Thomas for being the best brother I could ever ask for. I am also grateful for all the friends at home that stayed in touch the whole time.

TABLE OF CONTENTS

LIST OF FIGURES

LIST OF ACRONYMS/ABBREVIATIONS

1PA	One-photon absorption
2PA	Two-photon absorption
2PE	Two-photon emission
BBO	Beta barium borate
BD	Beam deflection
BS	Beam splitter
c.c.	complex conjugate
CA	Closed aperture
CA/OA	Closed aperture over open aperture
cm	centimeter
CPA	Chirped pulse amplification
CPM	Cross phase modulation
CS2	Carbon Disulfide
D-2PA	Degenerate two photon absorption
D-NLR	Degenerate nonlinear refraction
DFG	Difference frequency generation
DFWM	Degenerate four wave mixing

eV	Electronenvolt
fs	femtosecond
GVD	Group velocity dispersion
GVM	Group velocity mismatch
GW	Gigawatt
HW1/eM	Half width at 1/e maximum
HWP	Half wave plate
Hz	Hertz
m	meter
mJ	millijoules
mm	millimeter
ND-2PA	Nondegenerate two photon absorption
ND-NLR	Nondegenerate nonlinear refraction
NLA	Nonlinear absorption
NLR	Nonlinear refraction
nm	nanometer
OA	Open aperture
OPA	Optical parametric amplifier
OPG	Optical parametric generator

OR	Optical rectification
ps	picosecond
PSD	Phase sensitive detection
PW	Petawatt
QSE	Quadratic Stark effect
SFG	Sum frequency generation
SHG	Second harmonic generation
SPM	Self phase modulation
SVEA	Slowly varying envelope approximation
THG	Third harmonic generation
W	Watt
WLC	White light continuum
ZnO	Zinc oxide
ZnSe	Zinc Selenide

CHAPTER 1: INTRODUCTION

While optics is one of the oldest branches in physics with Ibn al-Haytham due to his ”Book of Optics” (1011-1021)[1] considered father of modern optics [2], the field of nonlinear optics is rather young. So it was in the 1930’s when Maria Göppert Mayer published her dissertation paper ”Über Elementarakte mit zwei Quantensprüngen” [42] to explain the simultaneous interaction of two light quanta. Showing generally, grounded on Diracs dispersion theory [43], the possibility of what has become known as two photon absorption (2PA) and emission (2PE), her publication laid the theoretical basis for nonlinear optics involving multi photon processes. So an excited atom can divide its excitation energy into two photons falling back to its ground state and vice versa two photons without sufficient energy to excite the atom on their own can still be absorbed as long as their energy sum is equal to the excitation energy of the atom (see figure 1 for the Jablonski diagrams).

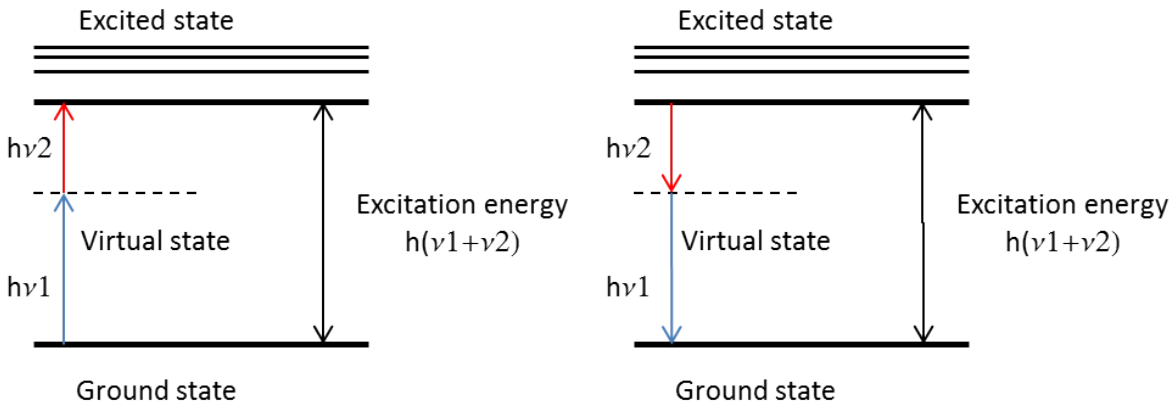

Figure 1.1: Jablonski diagrams for 2PA (left) and spontaneous 2PE (right)

The two step process, that is disconnected through a forbidden transition is modeled with an intermediate virtual energy state, a quantum state with very short life time. So as long as the electron

is found in the virtual state when the second photon hits it, 2PA is possible. Since these effects are possible, but very unlikely to happen with the provided light sources at time, experimental confirmation took another thirty years. This was achieved by Franken et al. (1961) [3] with their discovery of second harmonic generation (SHG) with in a quartz sample and even though the editorial journalist famously mistook the dim spot from the SHG as dirt and removed it from the publication, it still marks the beginning of experiments in nonlinear optics. The particular time for that to happen is not only by chance right after T. Maiman (1960) [4] successful ran the first laser in ruby crystal and was therefore responsible for an important step in the development of a new high intensity light source. Whereas for most light sources the polarization $P(t)$ of a material is approximately proportional to the electromagnetic field strength $E(t)$, laser light can generate sufficiently strong electromagnetic fields to enforce a nonlinear response of a material. In terms of M. Göppert Mayers description, that means the light quanta [42] flux density in the material is high enough to get a measurable count of 2PA processes despite the low probability for this interaction. But to stay with the little more plausible classical description, the incoming electromagnetic field displaces ions and electrons in a medium and generates so an oscillating polarization, which is phase shifted with respect to the driving field. This material polarization $P(t)$ can be expressed as a power series of the field strength $E(t)$

$$P(t) = \epsilon_0[\chi^{(1)}E(t) + \chi^{(2)}E^2(t) + \chi^{(3)}E^3(t)...] = P^{(1)} + P^{(2)} + P^{(3)}... \tag{1.1}$$

The quantities $\chi^{(1)}$, $\chi^{(2)}$ and $\chi^{(3)}$ are known as the first, second and third-order nonlinear optical susceptibility and are in general second rank, third rank and fourth rank tensors. Oscillating charges are also accelerated charges and therefore emit electromagnetic radiation again, that is now phase shifted compared to the incident radiation and phenomenological described by the refractive index. So it will be shown later, that the fourth rank tensor $\chi^{(3)}$ contributes and leads to an intensity

dependent refractive index.

$$n = n_0 + n_2 I \tag{1.2}$$

Consequences like for example self-focusing or self phase modulation make the study of nonlinear properties of material from a technical as well as from a scientific point of view quiet attractive. In recent years that caused the invention of several different techniques to determine nonlinear properties of material. In this work in particular the pump-probe and the Z-scan technique will be introduced and a the beam deflection technique will be applied in experiments on different samples. To accomplish a good evaluation on the presented technique, the samples CS_2, fused silica and ZnO cover a wide range of different material with respectively diverse optical response.

CHAPTER 2: THEORETICAL BACKGROUND

Linear Response

Optics is the subarea of physics that describes the propagation of light and its interaction with matter. As light is part of the electromagnetic spectrum and classical electromagnetism is completely described by the well known Maxwell laws, they are the foundation for most optical phenomena.

$$\nabla D = \rho_{free} \tag{2.1a}$$

$$\nabla B = 0 \tag{2.1b}$$

$$\nabla \times E = -\frac{\partial B}{\partial t} \tag{2.1c}$$

$$\nabla \times H = j_{free} + \frac{\partial D}{\partial t} \tag{2.1d}$$

Both the electric field E and the electric displacement D are appearing in those equations and they are linked due to the material equations.

$$D = \varepsilon_0 E + P \tag{2.2}$$

Considering just the linear response means the displacement of the electron by an electric field has to be sufficiently small and therefore the restoring force is proportional to the distance of displacement. In that case only the first term of $P(t)$ needs to accounted for. Using this aproximation is

leading to the wave equation

$$\nabla^2 E = \mu_0 \varepsilon_0 (1 + \chi^{(1)}) \frac{\partial^2 E}{\partial t^2} = \frac{\eta^2}{c^2} \frac{\partial^2 E}{\partial t^2} \tag{2.3}$$

with the complex index of refraction $\eta = n + i\kappa$. The real part of η defines the linear refractive index and determines the ratio between the vacuum speed of light and propagation speed through the medium. In combination with the absorption coefficient α, which is coupled to the imaginary part of the complex index of refraction, most common light matter interaction observations like absorption, refraction and reflection can be explained. For higher irradiance, however, the first order approximation is not sufficient to model the physical phenomena.

Nonlinear Response

To discuss the variety of second order order nonlinearities briefly, one can consider an incident optical field with two frequency components.

$$E(t) = E_1 e^{-i\omega_1 t} + E_2 e^{-i\omega_2 t} + c.c. \tag{2.4}$$

Taking only the assumed second order polarization into account.

$$P^{(2)}(t) = \varepsilon_0 \chi^{(2)} E(t)^2 \tag{2.5}$$

This leads to four different groups of polarization responses, Second-Harmonic Generation (SHG) $P(2\omega_1)$, $P(2\omega_2)$, Optical Rectification (OR) $P(0)$, Sum-Frequency Generation (SFG) $P(\omega_1 + \omega_2)$

and Difference-Frequency Generation (DFG) $P(\omega_1 - \omega_2)$. In a photon perspective SHG is illustrated as the creation of one photon with 2ω out of two photons with ω in a single quantum-mechanical process. It is most commonly used to convert the output frequency of a laser, which will be described in more detail at a later stage when the same mechanism is applied in the experiment. The same principle with just two different frequencies instead of twice the same is applied for SFG and DFG, who are the basis for Optical Parametric Amplifiers (OPA) and Optical Parametric Generators (OPG). In Contrast the emerging static term also known as optical rectification term does not lead to electromagnetic radiation generation, but creates a static electric field across the nonlinear crystal. Qualitatively different from these second order polarization responses are the nonlinear effects due to $P^{(3)}$

$$P^{(3)}(t) = \varepsilon_0 \chi^{(3)} E(t)^3 \tag{2.6}$$

For instance do third order nonlinear phenomena occur in media with and without inversion symmetry and are not vanishing like $\chi^{(2)}$ in centrosymmetric media. Again the third order processes can be distinguished in different classes to describe similar effects. For an incoming field with three different frequencies that leads to seven different nonlinear processes [6], Third-Harmonic Generation (THG), Self Phase Modulation (SPM) or Degenerate Nonlinear Refraction(D-NLR), Degenerate Two-Photon Absorption (D-2PA), Cross-Phase Modulation (CPM)or Nondegenerate Nonlinear Refraction (ND-NLR), Nondegenerate Two-Photon Absorption (ND-2PA), Degenerate Four Wave Mixing (DFWM), General Four Wave Mixing, Electric Field Induced Second-Harmonic Generation and the Quadratic Electro-Optical Effect. In this particular work, mainly ND-2PA and the connected Nondegenerate Nonlinear Refraction (ND-NLR) are of interest. For these nondegenerate effects two distinguishable beams are needed, and they are distinguishable either in direction

or frequency.

$$E_1(z,t) = \frac{1}{2}E_1(z)exp(\imath(k_1 z + \omega_1 t)) + c.c. \tag{2.7}$$

$$E_2(z,t) = \frac{1}{2}E_2(z)exp(\imath(k_2 z + \omega_2 t)) + c.c. \tag{2.8}$$

Substituting the resulting electromagnetic field into the wave equation

$$\nabla^2 E(z,t) - \frac{1}{c^2}\frac{\partial^2 E(z,t)}{\partial t^2} = \mu_0 \frac{\partial^2 P^{(3)}(z,t)}{\partial t^2} \tag{2.9}$$

leads to the described third order nonlinear phenomena and therefore to a polarization response at different frequencies. For NLA and NLR just consider the polarization terms at ω_1 and ω_2

$$P^{(3)}(z,t) = \frac{1}{2}(P_j(\omega_1)e^{\imath(k_1 z - \omega_1 t)} + (P_j(\omega_2)e^{\imath(k_2 z - \omega_2 t)} \tag{2.10}$$

with

$$P_j(\omega_1) = \frac{3}{4}\chi^{(3)}(\omega_1;\omega_1)|E_1(z,t)|^2 E_1(z,t)e^{\imath k_1 z} + \frac{6}{4}\chi^{(3)}(\omega_1;\omega_2)|E_2(z,t)|^2 E_1(z,t)e^{\imath k_1 z} \tag{2.11}$$

$$P_j(\omega_2) = \frac{3}{4}\chi^{(3)}(\omega_2;\omega_2)|E_2(z,t)|^2 E_2(z,t)e^{\imath k_2 z} + \frac{6}{4}\chi^{(3)}(\omega_2;\omega_1)|E_1(z,t)|^2 E_2(z,t)e^{\imath k_2 z} \tag{2.12}$$

The terms $\chi^{(3)}(\omega_1;\omega_1)$ and $\chi^{(3)}(\omega_1;\omega_1)$ are the degenerate susceptibilities referring to the self-induced nonlinearity, while the nondegenerate susceptibility $\chi^{(3)}(\omega_1;\omega_2)$ represents a nonlinearity induced in one beam due to another beam. Considering the polarization response of just one frequency, the wave equation is simplified

$$(\frac{\partial^2 E_1(z)}{\partial z^2} + 2\imath k_1 \frac{\partial E_1(z)}{\partial z}) = -\omega_1^2 \mu_0 P_j(\omega_1) e^{\imath \Delta k z} \tag{2.13}$$

With the Slowly Varying Envelope Approximation (SVEA)

$$\frac{\partial^2 E_1(z)}{\partial t^2} \ll 2k \frac{\partial E_1(z)}{\partial z} \tag{2.14}$$

and regarding phase matching condition $\Delta k = 0$ the equation can be rewritten

$$\frac{\partial E_1(z)}{\partial z} = \imath \frac{\omega_1}{8nc} (\chi^{(3)}(\omega_1;\omega_1)|E_1(z)|^2 E_1 + 2\chi^{(3)}(\omega_1;\omega_2)|E_2(z)|^2 E_1(Z)) \tag{2.15}$$

This can be separated into real and imaginary part by defining the complex electric field envelope as magnitude and phase term

$$E_1(z) = A_1 e^{\imath \phi_1(z)} \tag{2.16}$$

to

$$\frac{dA_1(z)}{dz} = -\frac{\omega_1}{8nc} Im(\chi^{(3)}(\omega_1;\omega_1) + 2\chi^{(3)}(\omega_1;\omega_2)) A_1(z)^3 \tag{2.17}$$

$$\frac{d\phi_1(z)}{dz} = \frac{\omega_1}{8nc} Re(\chi^{(3)}(\omega_1;\omega_1) + 2\chi^{(3)}(\omega_1;\omega_2))A_1(z)^2 \tag{2.18}$$

To define the two-photon absorption coefficient α_2 and the nonlinear index of refraction n_2, one needs to convert these equations to irradiance using

$$I(z) = \frac{1}{2} nc\varepsilon_0 A_1(z)^2 \tag{2.19}$$

and therefore

$$\alpha_2(\omega_1;\omega_i) = \frac{\omega_1}{2n^2c^2\varepsilon_0} Im(\chi^{(3)}(\omega_1;\omega_i)) \tag{2.20}$$

$$n_2(\omega_1;\omega_i) = \frac{1}{2n^2c\varepsilon_0} Re(\chi^{(3)}(\omega_1;\omega_i)) \tag{2.21}$$

Dependent on either degenerate or nondegenerate absorption and refraction, the index i gets the value 1 and 2. So the NLA and NLR is dependent on χ^3 a fourth rank tensor with 81 individual elements. Fortunately for most matter samples symmetric considerations help to reduce the number of independent tensor elements. However, the resulting polarization dynamics will be determined through the measurement.

Nonlinear Characterization Techniques

While the work is primarily concerned with beam deflection as method to characterize nonlinear properties of different material, there are other measurement techniques which will be described

briefly to compare them with the used technique.

Pump probe

One measuring method to determine dynamic absorption processes is the pump probe technique, illustrated in Figure 2. An intense pump is used to create a highly non-equilibrium state in the sample. The weaker probe beam does not have enough energy to change the properties of the excited material significantly, it therefore just experiences the absorption [7] or reflection [8] caused through the electrons in excited states.

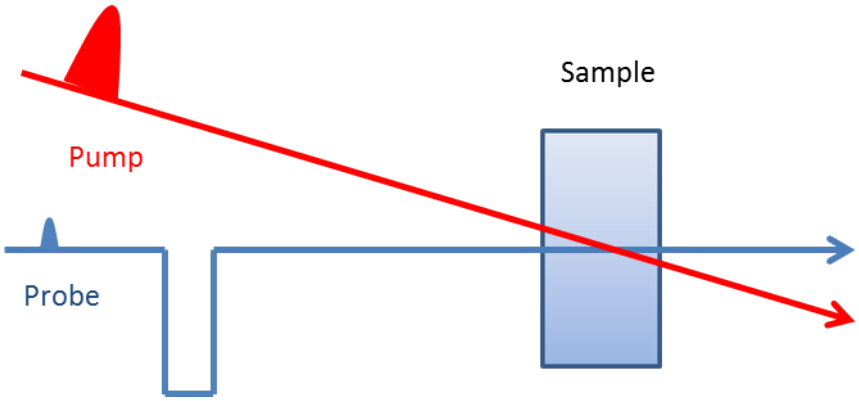

Figure 2.1: Pump Probe schematic

Using pulsed pump and probe allows the characterization of the time dynamics, measuring instantaneous and long lived effects. To do so the pulses are time delayed with respect to each other. The resolution hereby is limited due to the pulse width of the beam. Taking the general rate equations for the pump probe experiment

$$\frac{dI_p(z)}{dz} = -2\alpha_{2ND}(\omega_e, \omega_p)I_p(z)I_e(z) - \alpha_{2D}(\omega_p)I_p(z)^2 - \alpha(\omega_p)I_p(z) \tag{2.22}$$

$$\frac{dI_e(z)}{dz} = -2\alpha_{2ND}(\omega_e, \omega_p)I_p(z)I_e(z) - \alpha_{2D}(\omega_e)I_e(z)^2 - \alpha(\omega_e)I_e(z) \tag{2.23}$$

where the index p defines the probe terms and e the terms for the pump. Simplifying the equation according to the approximation that the probe is weak compared to the pump ($I_p(z) \ll I_e(z)$), the pump is undepleted ($dI_e(z)/dz = 0$), linear absorption is insignificant ($\alpha(\omega_p) = \alpha(\omega) \approx 0$) and there is no D-2PA resonance ($\alpha_{2D}(\omega_p) = 0$) leads to

$$\frac{dI_p(z)}{dz} = -2\alpha_{2ND}(\omega_e, \omega_p)I_p(z)I_e(z) \tag{2.24}$$

The system of equation can be solved [9] under the conditions that broadening during the propagation is negligible and pump as well as probe are transform limited pulses

$$Q(\sigma, \tau_{d,W,\rho,\Gamma}) = \frac{e^{-2\sigma}}{W\sqrt{\pi}} \int_{-\infty}^{\infty} (exp(-(\frac{\tau + \tau_d - \rho}{W})^2 - \frac{\Gamma\sqrt{\pi}}{\rho}(erf(\tau) - erf(\tau - \rho)))d\tau \tag{2.25}$$

with the normalized transmission $Q(\sigma, \tau_d, W, \rho, \Gamma)$, the 1PA cross section σ, the ratio $W = \tau_p/\tau_e$ of probe pulse width to pump pulse width, the two photon absorption parameter $\Gamma = LI_e\alpha_2$ and the group velocity mismatch ρ. While a quite capable technique to determine time dynamics of NLA, the pump probe setup is not able to determine NLR without some additional methods.

Z-Scan

Another technique and probably one of the mainly used one to determine nonlinear characteristics of materials is the by Sheik-Bahae et al. proposed Z-scan[10].

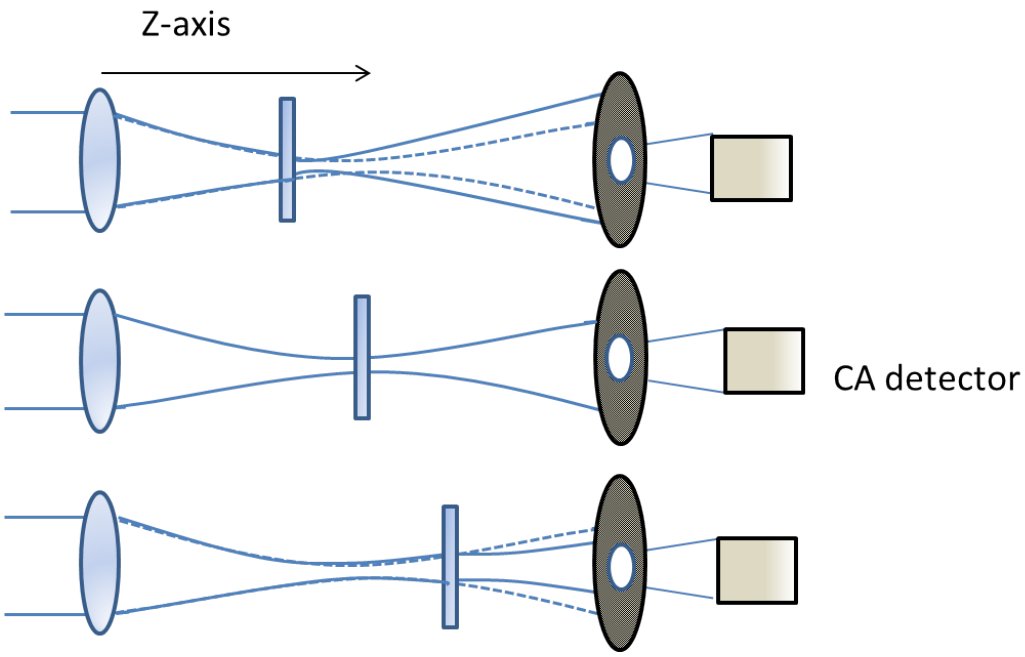

Figure 2.2: Z-scan schematic for positive nonlinear refractive index

One distinguishes between open aperture Z-scan (OA) and closed aperture Z-scan (CA). For both the sample gets moved through the focus of the beam along the z-axis and dependent on the z-position the intensity is recorded and compared to the reference arm (Figure 2.2). The OA determines the nonlinear absorption of the sample simply by collecting all the transmitted light after the sample. When the sample gets closer to the focal spot, the irradiance gets higher and therefore the absorption rises as well. To measure the nonlinear refractive index an additional aperture is placed at the far field of the beam, this setup (Figure 2.3) is than referred as closed aperture Z-scan (CA) and is based on the Kerr lens effect [11]. Since the refractive index is irradiance dependent, the sample acts as a lens inducing an extra phase front distortion of the incident beam [12]. A positive n_2 leads to a positive Kerr lens, which means that the sample is shifting the focal spot towards itself.

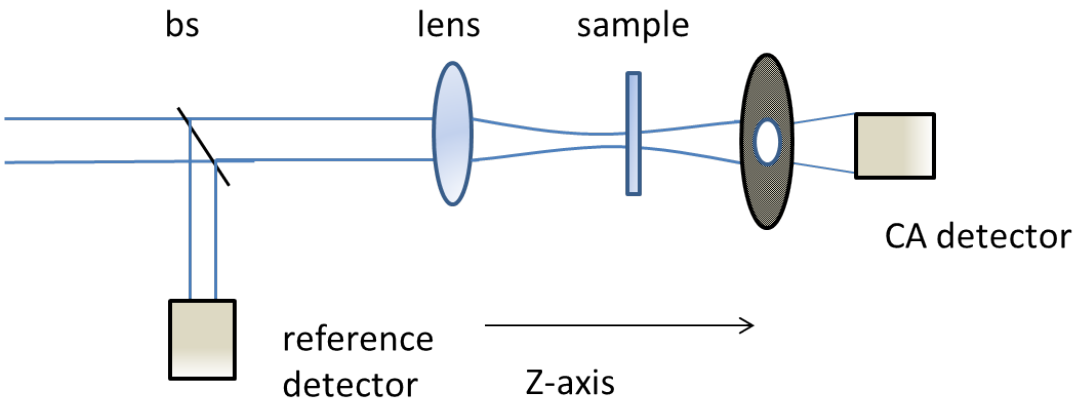

Figure 2.3: Closed Aperture Z-scan schematic

Therefore when the sample is placed before the beam focus, the new focal point will be further away from the aperture plane due the additional focusing power and the transmittance through the aperture decreases due to further beam expansion. On the other side of the beam focus the effect is similar leading to an opposite result. Again the new focal point is shifted closer to the sample but now closer to the aperture plane as well, hence the aperture transmittance increases. So for positive n_2, the on z-position dependent transmission results in a valley-peak shape, while a negative n_2 would result in a the reversed peak-valley shape. To fit the NLR measurement with the appropriate n_2 the presence of NLA and its influence on the CA measurement has to be considered. A simple division of the CA signal over the OA signal eliminates this distortion (Figure 2.4. This procedure, however, is misleading for high NLA and results in deceptive n_2 values [13]. While Z-scan is an effective technique to determine degenerate nonlinear properties, further adjustments need to be applied to measure nondegenerate nonlinear phenomena, time dynamics and anisotropy of nonlinearities. Examples for these extensions would be the two-color Z-scan [14] or the polarization Z-scan [15].

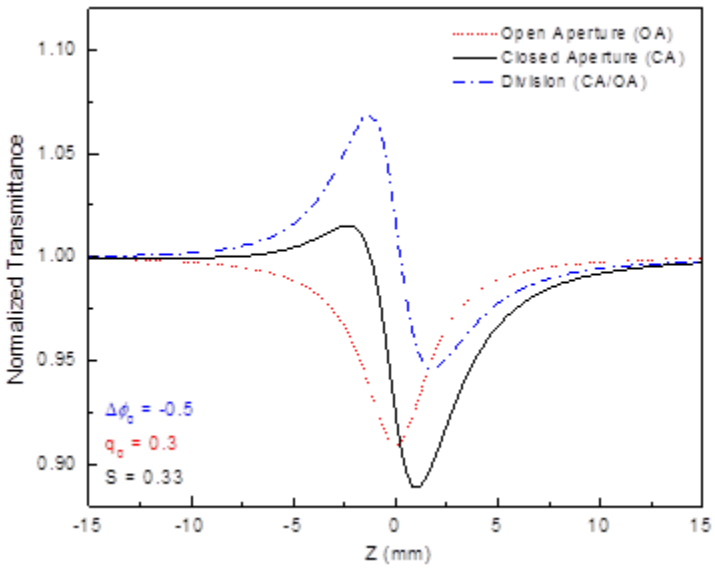

Figure 2.4: OA signal(red), CA signal (black) and Division CA/OA (blue) [16]

Beam deflection

As mentioned before, the single beam Z-scan is a simple and accurate working technique to determine degenerate nonlinear refraction and absorption. Measuring nondegenerate nonlinearities or their polarization dependence, however, requires more sophisticated experimental setups like the two-color Z-scan. Since this is a rather complicated and difficult experiment, a more straightforward and easier applicable technique is desirable. A known sensitive measurement tool to determine the absorption spectrum is the photothermal beam deflection initially developed by Boccara et al. [17]. Here the sample is illuminated by a strong pump beam and dependent on the absorption coefficient of the respective wavelength, the temperature of the tested material rises. The heat from the sample introduces a temperature gradient around the surface of the material, which further leads to a refractive index gradient in the adjacent air. This thermal dependence of the refractive index is commonly referred to as mirage effect an can be observed in daily life (e.g. streets in the sun)

While the pump beam is send directly through the sample, the probe propagates in the air along the surface and get deflected dependent on the to the absorption coefficient affiliated temperature change of the material. Following the basic idea and adding some modifications, the beam deflection principle will be used to measure ultrafast nonlinearities. So will both excitation and probe beam propagate through the sample and the refractive index gradient is generated not because of thermal energy, but nonlinear response instead.

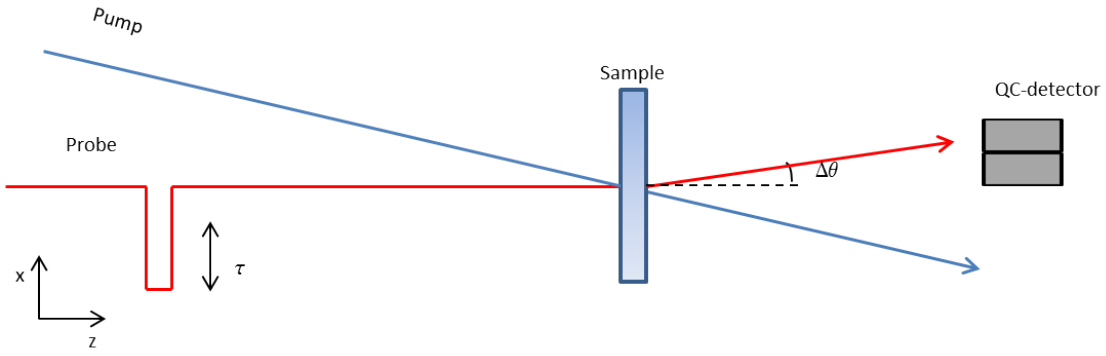

Figure 2.5: beam deflection schematic

To develop the theory for the beam deflection technique, one can start out with ray optics to analyze the pathway a beam is taking through an inhomogeneous medium with refractive index

$$n(\mathbf{r}) = n_0 + \Delta n(\mathbf{r}) \tag{2.26}$$

The Ray equation, which can be derived from Fermat's Principle [18], to describe the beam path can be simplified by considering small inhomogeneties $\Delta n(\mathbf{r} \ll n_0)$, only x components of the gradient of the refractive index $\Delta n(\mathbf{r}) = \Delta n(x)$ and small angles.

$$\frac{\partial}{\partial z}(n_0 \frac{\partial x}{\partial z}) \approx \frac{\partial \Delta n(x)}{\partial x} \tag{2.27}$$

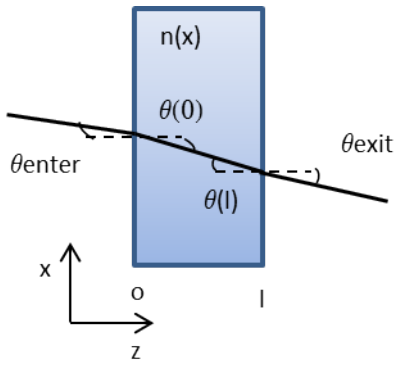

Figure 2.6: Model for deflection angle derivation

Because of the small angle approximation the equation can be rewritten, substituting $\theta_{in}(z) \approx \partial x/\partial z$

$$n_0(\frac{\partial \theta_{in}}{\partial z}) \approx \frac{\partial \Delta n(x)}{\partial x} \tag{2.28}$$

Integration over the length of the sample l yields

$$\theta_{in}(l) - \theta_{in}(0) = \frac{1}{n_0} \int_0^l \frac{\partial \Delta n(x)}{\partial x} \partial z \tag{2.29}$$

Following the derivation of Casperson [19] for photothermal beam deflection. The application of Snell's law gives the angle of the exiting beam and therefore the change of direction, due to the inhomogenous sample.

$$\Delta\theta = \theta_{exit} - \theta_{enter} = \int_0^l \frac{\partial \Delta n(x)}{\partial x} \partial z \tag{2.30}$$

While the deflection angle $\Delta\theta$ depends on the gradient of the refractive index , it does not so on the refractive index. This corresponds to ones perception, since a similar geometry with homogeneous sample obviously leads to equivalent entering and exiting angle.

Considering the simplified case without NLA and without any Group Velocity Mismatch (GVM), the two spatially and temporally Gaussian beams are propagated through the sample.

$$I_e(x, y, t) = I_{0,e} exp(-\frac{2(x^2 + y^2)}{w_e^2} - \frac{t^2}{\tau_e^2}) \tag{2.31}$$

$$I_p(x, y, z, t, \tau_d) = I_{0,p}(z) exp(-\frac{2(x^2 + y^2)}{w_p(z)^2} - \frac{(t - \tau_d)^2}{\tau_e^2}) \tag{2.32}$$

Where the excitation beam (index e) generates a refractive index gradient in the sample, that is experienced by the delayed (τ_d) probe beam (index p). The temporal pulse width τ and the spot size $w(z)$ are the the half width at $1/e$-maximum (HW1/eM) and I_0 the peak intensity. The simple adopted case can be approximated with the model of the earlier derived thin prism. The more general equation for the beam deflection angle transforms to

$$\Delta\theta = \int_0^l \nabla \Delta n_p(x, y, t) ds \tag{2.33}$$

A further assumption concerns the spot sizes of probe and pump beam. To obtain the maximum deflection, the index gradient has to be maximized as well. Therefore the spot size of the probe should be small and spatially shifted compared to the spot size of the pump (Figure 2.7).So the probe experiences an approximately linear index gradient in x-direction and a constant index in

y-direction. The change of index due to the intensity of the excitation beam in this model can be written as

$$\Delta n_p(x,y,t) = \Delta n_0 exp(-\frac{2(x^2+y^2)}{w_e^2} - \frac{t^2}{\tau_e^2}) \tag{2.34}$$

with Δn_0 as peak index change.

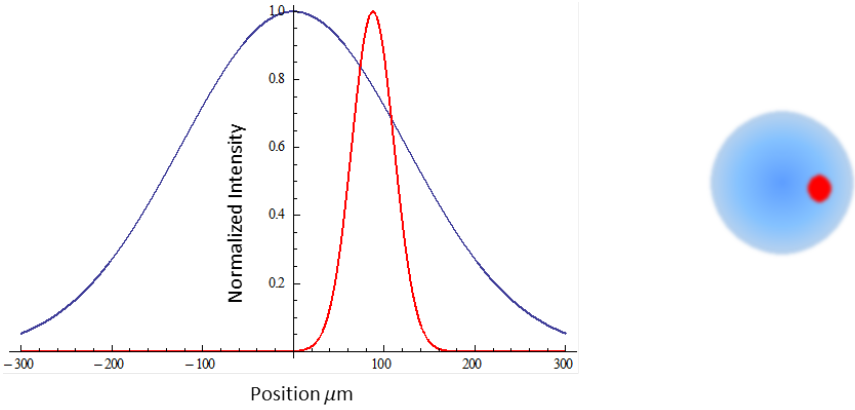

Figure 2.7: Position of probe $w_p = 33\mu m$ and pump $w_e = 175\mu m$, probe is shifted by $\frac{w_e}{2}$ for maximum deflection

Following the earlier outlined derivation, the beam deflection angle can be calculated as time dependent function.

$$\Delta\theta(w_e/2,0,t) = \frac{2L\Delta n_e}{w_0} exp(-\frac{1}{2} - \frac{t^2}{\tau_e^2}) \tag{2.35}$$

The deflected probe propagates the distance d to the detector, where the irradiance is expressed

as[20]

$$I_p(x,y,t,d) = I_{p,0}(d)exp(\frac{-2\pi^2 w_{p,0}^2((y-\Delta S(t))^2+x^2)}{d^2\lambda_p^2} - \frac{t^2}{\tau_p^2}) \tag{2.36}$$

considering wavelength λ_p, the beam waist $w_{p,0}$ and the pulse duration τ_p of the probe. Dependent on the distance between sample and detector and the beam deflection angle is the lateral shift $\Delta S(t) = d\theta(t)$ of the probe at the detector. Going further along with the derivation of Ferdinandus et al. [20], the measured power difference $\Delta P_p(t)$ between left and right side (x-direction) of the detector is determined due to integration over the x-y-plane of both sides

$$\Delta P_p(t) = \int_{-\infty}^{0}\int_{-\infty}^{\infty} I_p(x,y,t,d)dxdy - \int_{0}^{\infty}\int_{-\infty}^{\infty} I_p(x,y,t,d)dxdy \tag{2.37}$$

$$\approx P_{p,0}exp(-\frac{t^2}{\tau_p})\frac{2\sqrt{2}\pi w_{p,0}L}{\lambda_p w_e\sqrt{e}}\Delta n_p(t) \tag{2.38}$$

where $erf(x) \approx x$ as approximation for small x is used. To establish the NLR from the actual measured signal integrate over time

$$\frac{\Delta E_p}{E_p} = \frac{\int_{-\infty}^{\infty}\Delta P_p(t)dt}{\int_{-\infty}^{\infty}P_p(t)dt} = \frac{2\sqrt{2}\pi w_p L}{\lambda_p w_e\sqrt{e}}\langle\Delta n_p\rangle \tag{2.39}$$

with the sign of the NLR given by the sign of $\Delta E_p/E_p$ and $\langle\Delta n_p\rangle$ averaged index change over the probe irradiance. If the response times of the nonlinearities are much faster than the time duration

of the pump pulse, this can be rewritten as[20]

$$\frac{\Delta E_p}{E_p} = \frac{4L\sqrt{\frac{2\pi}{e}}w_{p,0}\Delta n_{p,0}}{w_e\lambda_p\sqrt{1+\frac{\tau_p^2}{\tau_e^2}}} \tag{2.40}$$

Now the nondegenerate bound electronic nonlinear refractive $2n_2(\lambda_p;\lambda_e)$ index is defined as $\Delta n_{p,0} = 2n_2(\lambda_p;\lambda_e)I_{e,0}$, so in cases with index changes merely due to electronic effects (i.e. bound electronic nonlinearity) it can be calculated directly from the signal $\Delta E_p/E_p$, which is proportional to the cross-correlation of excitation and probe pulses. For materials with an additional nonlinear refractive index change component due to non-instantaneous responses (e.g. due to nuclear movement) the signal is the convolution between response of the material and the cross-correlation of the pulses[20].

CHAPTER 3: EXPERIMENTAL APPARATUS

Laser system

For this experiment a complete Coherent Legend Elite system with Coherent Evolution pump laser and external Coherent Vitara-T seed laser was used to supply the necessary beams. The seed laser (Coherent Vitara-T) is a mode-locked solid-state laser with Ti:Sapphire as gain medium and semiconductor pump laser (Coherent Verdi G-Series) exciting at $532nm$. The titanium ions Ti^{3+} are responsible for the lasing while the sapphire Al_2O_3 is the substrate. Amplification of Ti:Sapphire is possible anywhere between $680nm$ and $1100nm$, but the reflectivity of the optics in the cavity restrict the wavelength range here from $755nm$ to $860nm$. To create ultrashort pulses the Vitara-T applies Kerr lens modelocking as a passive modelocking technique. In contrast to active modelocking setups no additional external signal is needed. A change of intensity leads to a change of refractive index in material, which is also known as the optical Kerr effect [5]. Therefore fluctuations in light intensity vary the beam diameter in the cavity as well. The Gaussian pump mode distribution with high gain in the center and low gain at the edges of the gain medium works as soft aperture. So the relatively low intensity continuous wave mode with big diameter experiences less gain than high intensity pulse. This dominant pulse then forms the output. While once started, the pulsed mode continues running by itself, but in order to get high enough fluctuations to cause Kerr lensing a starting mechanism is needed. In the Coherent Vitara-T this is achieved by changing the cavity length at proper speed [23]. The output of this seed laser is propagated to the Coherent Legend Elite amplifier and due to chirped pulse amplification (CPA) amplified. The setup of the Coherent Legend Elite basically consist of Coherent Evolution pump laser, stretcher, regenerative amplifier and compressor [24]. CPA was developed from D. Strickland and G. Mourou 1985 [25] and is a technique to circumvent the amplification limit in consequence of the destruction threshold

of the gain medium. To realize that, the stretcher introduces a phase whose time derivative is not constant, known as group velocity dispersion (GVD), on the pulse. Therefore the pulse is chirped and its time duration is longer. A femtosecond pulse can be broadened up to a factor of 10^4 with this technique [26]. Energy conservation now dictates a decrease of amplitude of the stretched pulse. The longer and decreased (amplitude) pulse can be amplified again without destroying the gain medium due to the peak intensities. The Coherent Legend Elite amplifies the pulse by a factor of around 10^6 [24]. To get the original pulse duration back, the compressor introduces an additional phase with opposing sign, which eliminates the GVD and therefore shorten the pulse again.

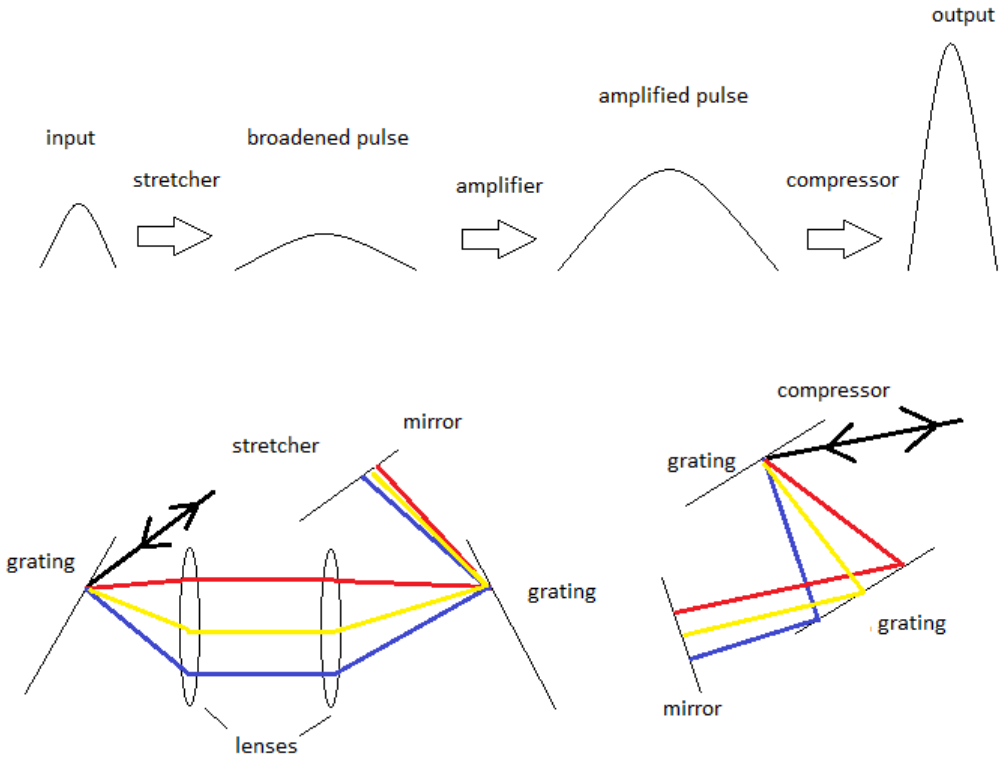

Figure 3.1: Basic functionality schematic for CPA and possible arrangement for each the stretcher and the compressor, in the stretcher sketch shorter wavelength are propagating through a longer path and will be delayed, the compressor on the other hand introduces the opposite effect and eliminates the GVD again

There are different possible setups to achieve pulse stretching and compression. The Coherent Legend Elite uses diffraction gratings similar to the sketches in Figure 3.1, where the positioning of the grating is crucial to avoid angular chirp [27]. Amplification between stretcher and compressor is done with two Ti:Sapphire crystals, one used as single-pass amplifier stage and the other one working as regenerative amplifier. As result an output of pulses with pulse width smaller than $25fs$ and pulse energies bigger than $12mJ$ at a central wavelength of $800nm$ can be achieved [28]. The specific parameters for the experiments are measured independently and will be stated in the relevant chapter.

Optical Setup

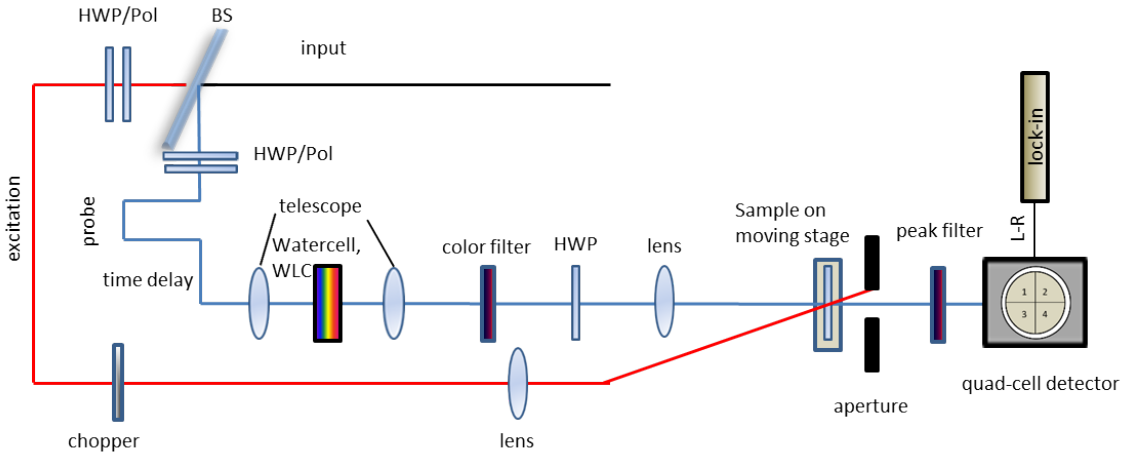

Figure 3.2: Experimental setup schematic

The incoming beam is separated due to the beam splitter (BS) into excitation and probe beam. Both beams are send through a combination of half-wave plate (HWP) and polarizer to control and manipulate their polarization and pulse energy. To measure the temporal response, there is a delay stage set up in the probe path. Also as mentioned earlier, to satisfy the condition that the spot size

of the probe needs to be smaller than the one of the excitation beam, a telescope is installed. Inside the telescope is a water cell to generate a white light continuum (WLC) from the femtosecond laser pulses. While a complete theory of WLC generation is still considered one of the bigger unsolved problems in nonlinear optics, it seems that pulse self-steepening [29] leads to optical shock-wave formation [30] and is therefore the physical reason for WLC generation. Although an accurate model description of WLC generation is not necessary here, since it is merely an instrument to get different wavelengths, what happens to a short intense pulse propagating through a nonlinear medium is a significant spectral broadening. This effect was first discovered by Alfano and Shapiro in 1970 [31]. Even though the temporal coherence of the new pulse is low (broad spectral bandwidth), the spatial coherence remains high. Dependent on the desired wavelength range, the broadened probe pulse is filtered by a specific color filter. For the experiment with Zinc Oxide the water cell was substituted with a barium borat BBO crystal to generate the probe with second harmonic generation (SHG). SHG can be understood in a photon view as the summation of two photons with energy $\hbar\omega$ to one photon with energy $2\hbar\omega$. Because of symmetry conditions, the second harmonic can just be generated in optical anisotropic material. Also phase matching conditions inside the material have to be met. In the former considered photon view, that simply means conservation of momentum. This translates to the more practical electromagnetic wave perception to equal phase velocities of exciting wave and second harmonic. In general the condition is not fulfilled, since the refractive index is wavelength dependent. With the aid of birefringent crystals, where the refractive index is also dependent on the polarization of the electromagnetic wave, phase matching is achievable. The index ellipsoid for the uniaxial BBO to calculate the phase match angle θ_m, can be expressed as

$$\frac{1}{n_o(\omega)^2} = \frac{sin^2(\theta_m)}{n_e(2\omega)^2} + \frac{cos^2(\theta_m)}{n_e(2\omega)^2} \tag{3.1}$$

with the ordinary n_o and the extraordinary n_e refractive index. Simple trigonometry leads to the resulting phase matching angle

$$sin^2(\theta_m) = \frac{\frac{1}{n_o(\omega)^2} - \frac{1}{n_o(2\omega)^2}}{\frac{1}{n_e(2\omega)^2} - \frac{1}{n_o(2\omega)^2}} \tag{3.2}$$

Applied on the SHG in the experiment from $800nm$ to $400nm$, the angle is $\theta_m = 13,57°$ calculated from Sellmeier equation with the values of Kato [39]. Going further along the setup, another HWP is used to change the polarization of the probe with respect to the pump. To adjust the polarization an additional polarizer set perpendicular to the desired polarization direction is placed in the beam path. Minimizing the probe with the HWP leads to the required polarization. Both probe and excitation beam are then focused on the sample, with the smaller probe hitting the sample straight and shifted spatially to one of the slopes of the excitation beam (see figure 2.7). The excitation is also modulated at $286Hz$ with a mechanical chopper and synchronized with the lock-in amplifier to eliminate most of the noise, before it gets focused on the sample. To hold the sample, it is mounted on a movable 3-D stage, which allows precise translation in all directions. The same stage is also used for the knife edge scan to determine the spot sizes of the probe and the excitation beam. Hereby the sample is exchanged with a knife edge and moved on the translation stage through the beam (see figure 3.3). The transmitted power is measured as the knife cuts through the beam. With known beam profile this measurement leads to the spot size of the probe and the excitation.

Finally there is the signal detection and data acquisition part of the experimental setup, which is shielded by an aperture and a peak filter to keep the noise level low. It consists of a quad cell detector and a lock-in amplifier, who are described more rigorous in the next section.

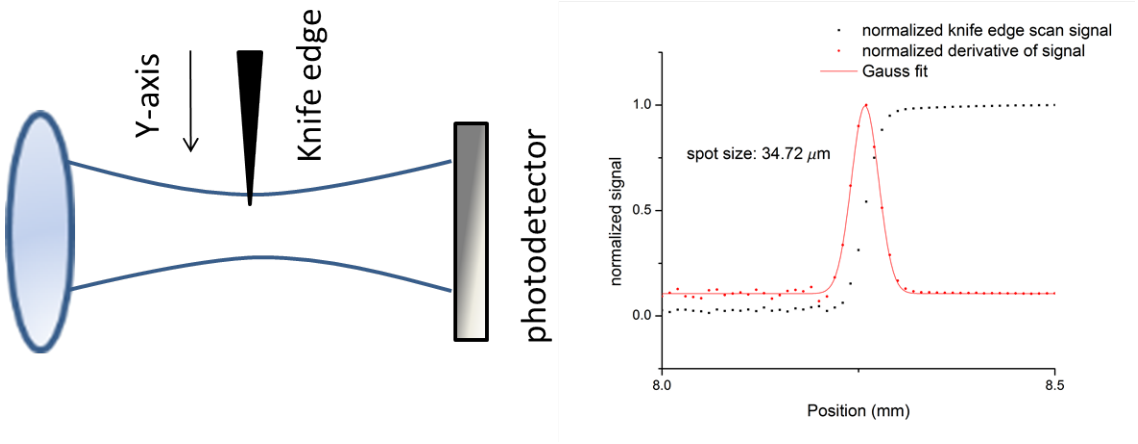

Figure 3.3: knife edge schematic (left) and graphical analysis of the probe (right)

Detection

The signal detection in this experiment acquires high sensitivity to measure small nonlinearities. It consists of an OSI Optoelectronics QD50-0-SD quad-segment diode and Stanford Electronic SR830 digital and SR510 analog lock-in amplifiers to handle the diodes output and digitize it by a National Instrument data acquisition card.

Quad cell detector

The principle of quadrant-cell photodiodes is based on separation of the photoactive areas. These four photodiode elements are isolated by a small gap and the anode of each element is separately available. Therefore the energy distribution of a light spot over the diode segments can be measured and its relative position with respect to the center of the detector determined. The four independent current outputs are then converted to voltage using four transimpedence amplifiers and further

processed to yield three voltage outputs.

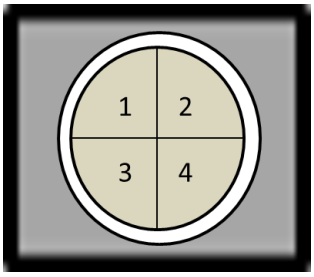

Figure 3.4: Quad cell detector schematic

The difference between left and right

$$\Delta U_{L-R} = (U_1 + U_3) - (U_2 - U_4) \tag{3.3}$$

between top and bottom

$$\Delta U_{T-B} = (U_1 + U_2) - (U_3 + U_4) \tag{3.4}$$

and the total voltage

$$U_t = U_1 + U_2 + U_3 + U_4 \tag{3.5}$$

where the index number refers to the segment number in figure 3.4. Also an amplification gain of 10^4 on the voltage is applied through the first transimpedance stage[21]. Exercising simple

arithmetic on the output voltages gives the x and y position of the spot

$$x = \frac{U_{L-R}}{U_t} \tag{3.6}$$

$$y = \frac{U_{T-R}}{U_t} \tag{3.7}$$

which is the critical information in the experiment.

Lock-In Amplifier

Precise measurements of small AC signals in the presence of strong noise sources can be done with Lock-in amplifiers. Hereby a technique known as phase-sensitive detection (PSD) is applied to isolate the signal and get rid of the noise at different frequencies[22]. In our case the signal of the probe is modulated with a mechanical chopper, to generate the necessary reference frequency. The signal $U_{sig}sin(\omega_r t + \theta_{sig})$ can be defined through the amplitude U_{sig}, the signal frequency ω_r and the phase θ_{sig}. Using PSD the signal is multiplied with the lock-in amplifiers own internal signal $U_L = sin(\omega_L t + \theta_L)$, which is just the product of two sine waves

$$U_{psd} = U_{sig}U_L sin(\omega_r t + \theta_{sig})sin(\omega_L t + \theta_L) \tag{3.8}$$

$$= \frac{1}{2}(U_{sig}U_L cos((\omega_r - \omega_L)t + \theta_{sig} - \theta_L) - U_{sig}U_L cos((\omega_r + \omega_L)t + \theta_{sig} + \theta_L)) \tag{3.9}$$

So there are two output signals of the PSD, one at the sum frequency $\omega_r + \omega_L$ and another one at

the difference frequency $\omega_r - \omega_L$. Applying a low pass filter on the PSD output removes the AC signals and there won't be anything left unless the two frequencies ω_r and ω_L are equal. Thus the difference frequency component will be a DC signal and pass the low pass filter.

$$U_{psd} = \frac{1}{2} U_{sig} U_L cos(\theta_{sig} - \theta_L) \tag{3.10}$$

Considering signal and additional noise,instead of a simple sine wave, the combination of PSD and low pass filter only detects the signals with frequencies close to the internal lock-in reference frequency. Since the noise is distributed over a wide range of frequencies, most of it gets attenuated. The hereby for signal detection used Stanford Systems SR830 lock-in amplifier is a digital lock-in, where multiplication and filtering is done mathematically using a digital signal processing chip.

Experimental Procedure

The first step of the experiment is placing the sample at the beam waist of the probe. Therefore $ZnSe$ a material with large NLA is used to conduct an OA Z-scan. The beam waist is found at the position of minimum transmission. To determine the spot sizes of probe and pump, the $ZnSe$ is exchanged with a knife edge and a knife edge scan is done at the beam waist. For good responsivity and linearity of the gradient index, the ratio between probe waist w_p and excitation waist w_e should be set from 2 to 5 [20]. The telescope allows adjustments of the spot size of the probe. With the long lifetime nonlinear absorber $SiNC$ zero time delay can be found and therefore the position where the maximum signal is expected. After replacing the $SiNC$ with the sample, the position of the detector can be adjusted. So propagating just the probe should give no signal on the quad cell detector for left-right or top-bottom. To get an optimal signal the pump direction is adjusted until the maximum left-right signal is observed, which corresponds to the highest index gradient(see

figure 2.7). After finishing the temporal and spatial alignment, the left-right signal is recorded while the delay stage in the probe path is scanned to deliver different temporal delay between probe and excitation. As first sample fused silica is used to calibrate and reassess the experiment. In addition the setup allows changing the polarization of the probe compared to excitation (see optical setup for more details).

CHAPTER 4: RESULTS

Fused Silica

Fused Silica is melted natural crystal quartz and so glass consisting of silica in amorphous form. It has a macroscopic inversion symmetry that does not allow second order nonlinear processes [32]. The ultrafast purely electronic nonlinear response in this isotropic medium, allows the verification of the calibration of the experimental setup on the one hand and the determination of the probe pulse duration on the other hand. Due to the ultrafast electronic response, the beam deflection signal results in the cross correlation between the probe pulse and the excitation pulse.

$$S(\tau) = \int_{-\infty}^{\infty} I_e I_p(t-\tau)dt \tag{4.1}$$

Examining the Fourier transformation of the signal yields

$$F[S(\tau)] = S(\omega) = I_e(\omega) I_p(\omega) \tag{4.2}$$

Taking into account Gaussian shapes for signal (see figure 4.1), excitation and probe pulse, it leads to $\tau_{cross}^2 = \tau_e^2 + \tau_p^2$ as relation between the pulse widths. The signal width τ_{cross} is determined in this measurement, while the excitation width $\tau_e = 47fs$ is known due to earlier auto correlation measurements in order to characterize the laser output. The probe widths τ_p, which is influenced by the WLC generation and the following color filter and is different from the excitation width, can be calculated using the signal width. The calibration measurement is done with a sample of fused silica with length $L = 1mm$ and co polarized excitation and probe (Figure 4.1).

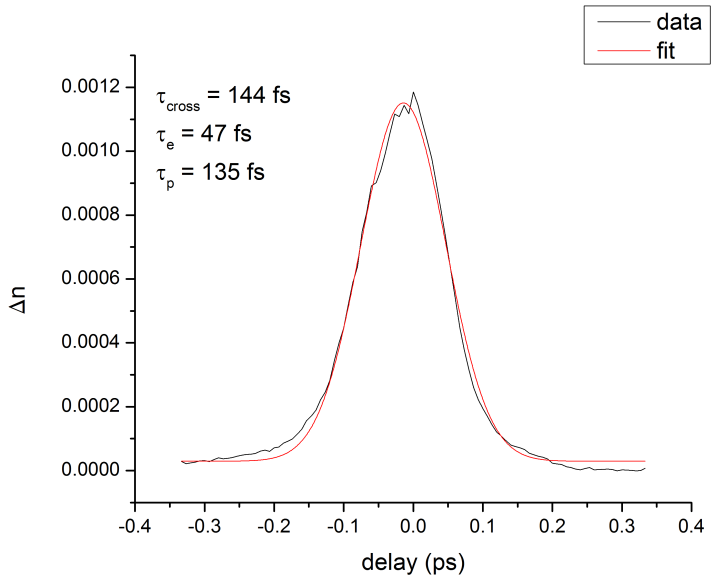

Figure 4.1: Measured index change Δn dependent on the delay in fused silica for the co polarized case with $L = 1mm$, $\lambda_e = 800nm$, $\lambda_p = 650nm$, $w_e = 175\mu m$, $w_p = 43\mu m$, $\tau_e = 47fs$, $\tau_p = 135fs$ and $I_e = 1,63PW/m^2$

The pulse width of the probe is determined with the measurement and results to $\tau_p = 135fs$. Following the early thin sample derivation and recognizing the peak index change $\Delta n = 0.00119$, the nonlinear refractive index of fused silica

$$\Delta n_p = 2n_2(\lambda_p; \lambda_e)I_e \tag{4.3}$$

is calculated as $n_2 = 0,26 \times 10^{-19} \frac{m^2}{W}$ which is consistent with the literature value [33]. This calibration is performed before every measurement and the just realized measurement is used for the CS_2 experiment. But before going more into detail about Carbon Disulfide next chapter, the co and cross polarized cases (polarization direction between probe and excitation) are measured for fused silica. The nonlinearity in fused silica is purely electronic and as stated earlier, it is an

isotropic material which leads to the third order susceptibility relations $\chi_{1111} = \chi_{1122} + \chi_{1212} + \chi_{1221}$, since isotropic nonlinearities should be invariant to rotation of the material. In the Kleinman limit the susceptibility elements are related by $\chi_{1122} = \chi_{1212} = \chi_{1221}$ [5]. Therefore the ratio of the susceptibilities and following the peak index changes $\Delta n_{co}/\Delta n_{cross} = \chi_{1111}/\chi_{1122} = 3$.

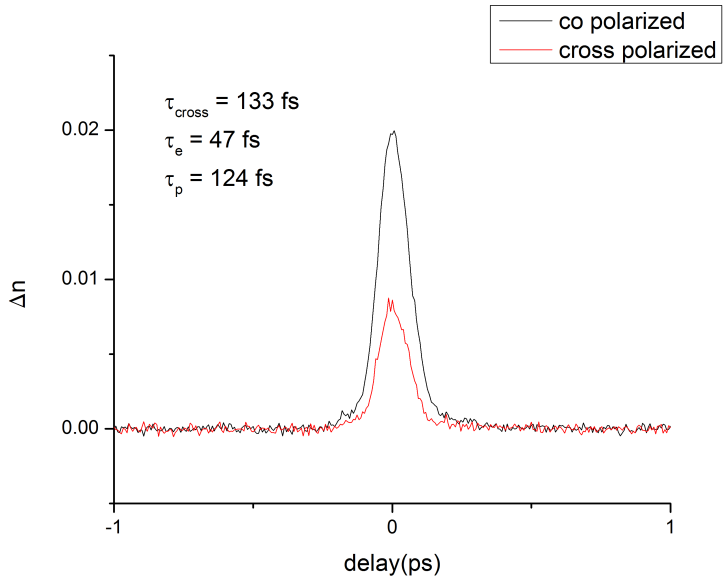

Figure 4.2: Measured index change Δn dependent on the delay in fused silica for the co (black) and cross (red) polarized case with $L = 1mm$, $\lambda_e = 800nm$, $\lambda_p = 650nm$, $w_e = 175\mu m$, $w_p = 43\mu m$, $\tau_e = 47fs$, $\tau_p = 124fs$ and $I_e = 0,43PW/m^2$

For the co polarized case a peak index change of $\Delta n = 1,99 \times 10^{-2}$ and for the cross polarized case the value $\Delta n = 0,78 \times 10^{-2}$ are observed (see figure 4.2. This leads to a measured ratio $\Delta n_{co}/\Delta n_{cross} = 2,5$ which is considering particularly the noise level on the peak a satisfying result.

Carbon Disulfide

Carbon Disulfide CS_2 is a material where the characterization of the nonlinear refractive index is studied exhaustively. The reason for the uninterrupted interest in the linear diatomic liquid

$$S = C = S \tag{4.4}$$

is the compared to other liquids large nonlinear refractive index [34], which leads to a wide range of applications like optical switching [35] and limiting [36]. Also the wide transparency range over the visible and infrared region [37] make CS_2 a neat liquid to work with. As mentioned earlier, before the temporal response of CS_2 is measured and therefore the non-instantaneous components are determined, the calibration with fused silica has to be done (see figure 4.1). The first measurement of CS_2 can be seen in figure 4.3.

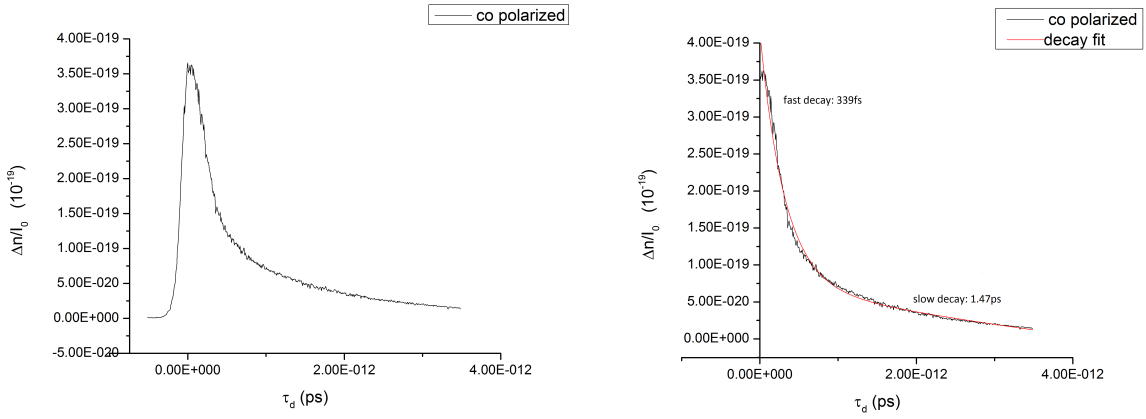

Figure 4.3: Measured index change Δn over excitation intensity versus time delay for the co polarized case with $L = 1mm$, $\lambda_e = 800nm$, $\lambda_p = 650nm$, $w_e = 175\mu m$, $w_p = 43\mu m$, $\tau_e = 47fs$, $\tau_p = 135fs$ and left fit of the decay

The decay of the curve reveals two temporal components, that could not been observed in fused silica. Separate exponential fitting of the two decays lead to a time constant of $339fs$ for the fast response and $1,47ps$ for the slow response. The reason for the slow response lies in the molecular reorientation relaxation process. By applying an electric field to the liquid, the molecules become aligned alongside it. Therefore the probe experiences a changed value for the refractive index. Through thermal movement, that randomizes the molecular orientation, the modification is reversed as the electric field weakens. Compared to the instantaneous electronic response or the fast response which is probably a combination of molecular libration, a bound electronic response ($< 170fs$) and inter molecular response ($400 - 600fs$) [20], the reorientation is relatively slow. The determined value is within the scope of the literature value [5], considering the slight influence the other material responses still at the later times and the noise level. A separation of the fast responses is not possible due to the pulse duration of probe and excitation. Having looked upon the time dynamics, another dependency of the nonlinear refractive index, the polarization dependency, can be examined with the experimental setup. This is performed using three different polarization angles between excitation and probe, $0°$ (co polarized), $90°$ (cross polarized) and $54,7°$ (the magic angle) (see figure 4.4). The magic angle is a special angle, where the index change through reorientational response is zero. Since the molecules are oriented randomly, they contribute to the index change either increasing or decreasing. At the magic angle, however, the average angular dependence goes to zero, which eliminates the reorientational response. To evaluate the results, the responses can be decomposed in isotropic and reorientational responses with respect to the polarization angle.

$$\Delta n(\theta) = \Delta n_{iso}(cos^2(\theta) + \frac{1}{3}sin^2(\theta)) + \Delta n_{re}(cos^2(\theta) - \frac{1}{2}sin^2(\theta)) \tag{4.5}$$

While the factor for the isotropic nonlinearity is already described at the previous section with

fused silica, is the index change of the cross polarized case negative one half of the co polarized one.

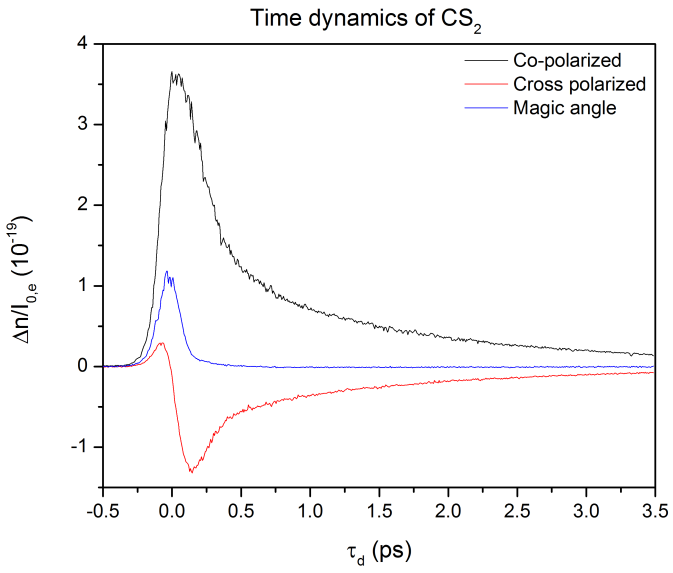

Figure 4.4: Measured index change Δn over excitation intensity versus time delay for the co polarized (black), cross polarized (red) and magic angle (blue) case with $L = 1mm$, $\lambda_e = 800nm$, $\lambda_p = 650nm$, $w_e = 175\mu m$, $w_p = 43\mu m$, $\tau_e = 47fs$, $\tau_p = 135fs$

This can be explained that only the molecules in the plane of the exciting electric field are turned away from the probe in the cross polarized case, whereas in the co polarized case all molecules are turned towards the probe. Considering uniformly distributed molecules in all direction, averaging results in the factor $-1/2$, with the minus sign taking into account the decreasing effect. The application of this equation for the three different responses, leads to the relations for co polarized($0°$), cross polarized ($90°$) and magic angle ($54,7°$)

$$\Delta n_{co} = \Delta n_{iso} + \Delta n_{re} \tag{4.6}$$

$$\Delta n_{cross} = \frac{1}{3}\Delta n_{iso} - \frac{1}{2}\Delta n_{re} \tag{4.7}$$

$$\Delta n_{magic} = \frac{5}{9}\Delta n_{iso} \tag{4.8}$$

While the magic angle has no reorientational nonlinearities, the slow responses of the co and the cross polarized measurements should be in a ratio of -2 and can therefore be compared by applying the factor on the sampled data. One can recognize in figure 4.5 the responses match as expected. In particular at later times, where the influence of the fast electronic response vanishes, the two graphs match exactly.

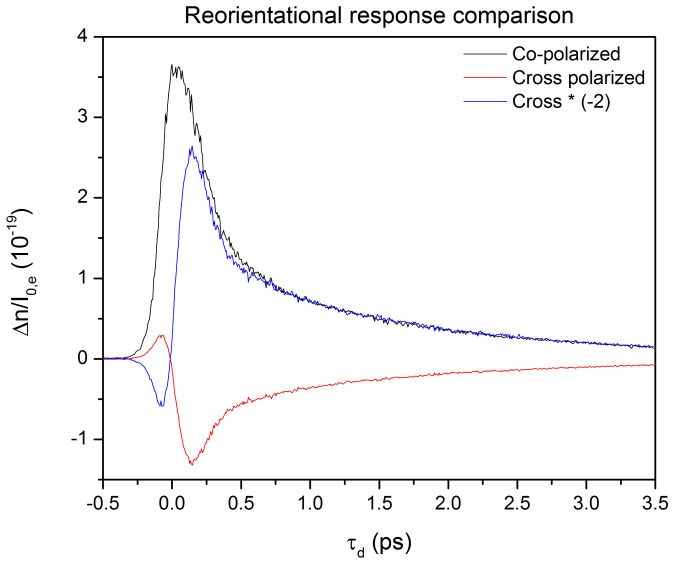

Figure 4.5: Measured index change Δn over excitation intensity versus time delay for the co polarized (black), cross polarized (red) and cross polarized with applied factor -2 (blue) to compare the reorientational nonlinearities with $L = 1mm$, $\lambda_e = 800nm$, $\lambda_p = 650nm$, $w_e = 175\mu m$, $w_p = 43\mu m$, $\tau_e = 47fs$, $\tau_p = 135fs$

To determine the isotropic and the reorientational contribution, the magic angle response can be scaled with $9/5$ and the here gained isotropic contribution subtracted from the co polarized response

$$\Delta n_{re} = \Delta n_{co} - \Delta n_{iso} = \Delta n_{co} - \frac{9}{5}\Delta n_{magic} \tag{4.9}$$

which leads to the reorientational contribution. The result of this analysis can be seen in figure 4.6.

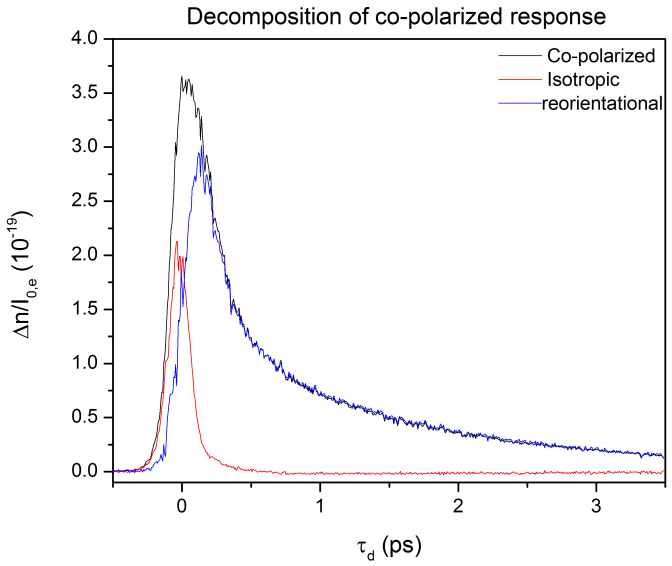

Figure 4.6: Measured index change Δn over excitation intensity versus time delay for the co polarized (black) and decomposition in its isotropic(red) reorientational contribution(blue) with $L = 1mm$, $\lambda_e = 800nm$, $\lambda_p = 650nm$, $w_e = 175\mu m$, $w_p = 43\mu m$, $\tau_e = 47fs$, $\tau_p = 135fs$

Now that the reorientational and the isotropic contributions of the nonlinear index change of CS_2 are determined, one should be able to reconstruct the response at any given polarization angle using the earlier stated equation. This reconstruction is performed with the cross polarized measurement, which was not part of the decomposition and is therefore an independent instance to check the

assumption of just two response sources (isotropic and reorientational).

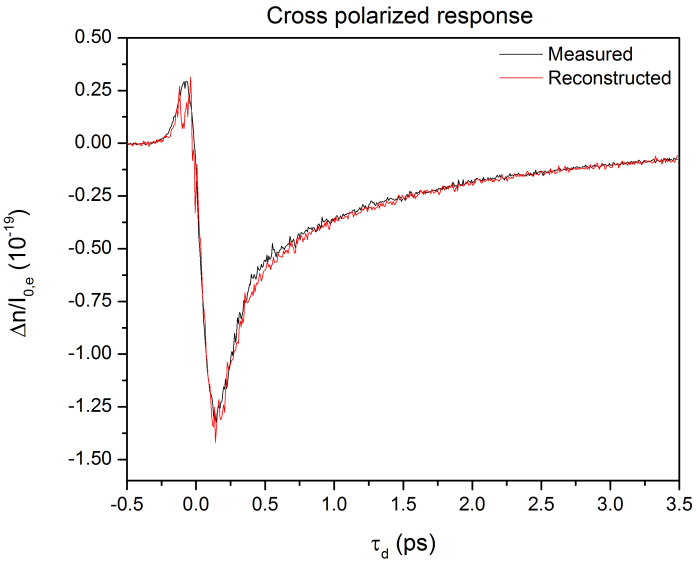

Figure 4.7: Measured index change Δn over excitation intensity versus time delay for cross polarization (black) and reconstruction from the isotropic and reorientational contributions(red) $L = 1mm$, $\lambda_e = 800nm$, $\lambda_p = 650nm$, $w_e = 175\mu m$, $w_p = 43\mu m$, $\tau_e = 47fs$, $\tau_p = 135fs$

This reconstruction (see figure 4.7) works pretty well and verifies the model. Small differences between measurement and reconstruction may be through small errors in the polarization angle settings. These are adjusted manually and are therefore just accurate about 1 degree. Also it is believed that the nuclear response has an isotropic angular dependence, that cannot be resolved with the given pulse duration.

Zinc Oxide

Zinc Oxide is a direct wide band gap semiconductor with a band gap of $3.37eV$ $(368nm)$ at room temperature. Optical properties of semiconductors are dependent on intrinsic and extrinsic effects.

The optical transitions between electrons in the conduction band and holes in the valence band are hereby defined as intrinsic, while dopants in the band gap influencing absorption and transmission are extrinsic [38]. As material with large NLR, 2PA and not negligible group velocity mismatch (GVM) and group velocity dispersion (GVD), ZnO can be considered a significant test of beam deflection as technique to measure nonlinear properties. Other than in the previous measurements, the probe is not generated from WLC but as earlier described due to SHG in a BBO-crystal. Therefore a new calibration with fused silica has to be performed, to determine the new probe pulse width (see figure 4.8).

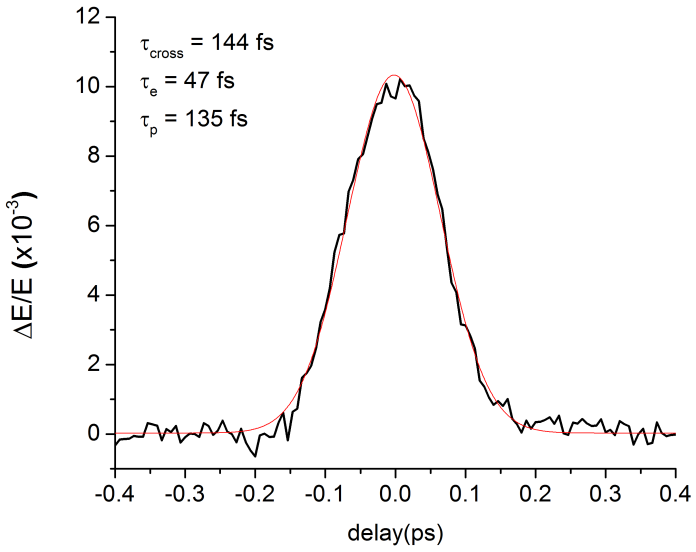

Figure 4.8: Beam deflection measurement with fused silica for calibration, data(black) and fit(red) $L = 1mm$, $\lambda_e = 800nm$, $\lambda_p = 400nm$, $w_e = 178\mu m$, $w_p = 45\mu m$, $\tau_e = 47fs$, $\tau_p = 100fs$

To measure the 2PA, the experimental setup is changed to a pump probe setup. So the probe is not spatially shifted compared to the probe anymore and the detector records the total signal instead of an left minus right signal. This is done for three different excitation pulse energies and the transmission curves dependent on the time delay can be seen in figure 4.9. One can recognize in

all three curves, that what is supposed to be the maximum absorption peak at zero delay time, is an absorption plateau instead. Since the ZnO sample has a finite thickness ($L = 0,53mm$) and the probe pulse ($400nm$) moves, because of GVM, slower through the sample than the excitation pulse ($800nm$), the excitation pulse can overtake the probe pulse inside the sample. That means different delay times actually lead to perfect temporal overlap at different positions inside the sample and therefore to the absorption plateau. Also, because the band gap is bigger than the photon energy of the excitation beam, the nonlinear responses have to involve virtual processes leading to just instantaneous responses.

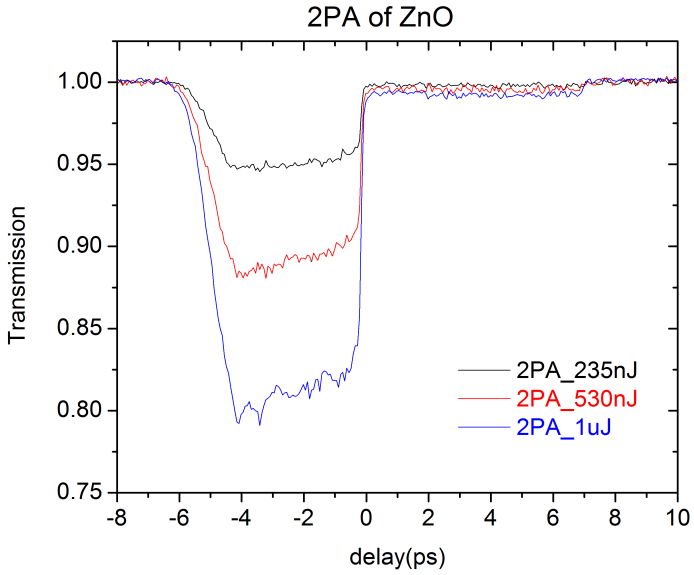

Figure 4.9: Total transmission in ZnO for three different excitation pulse energies $235nJ$(black), $530nJ$ (red) and $1000bJ$ (blue) $L = 0,53mm$, $\lambda_e = 800nm$, $\lambda_p = 400nm$, $w_e = 178\mu m$, $w_p = 45\mu m$, $\tau_e = 47fs$, $\tau_p = 100fs$

For the same three excitation pulse energies the beam deflection is performed as well (see figure 4.10). It is similarly to the absorption curves evident, that the slope for negative time delay is not as steep as for zero delay. Since negative delay means the probe reaches the sample before the

excitation and the two pulses meet on the back of the sample, due to the path through the material with GVD both pulses get temporal broadened and so lead to the slower response. Fitting the data for transmission and beam deflection yields the average determined nonlinear absorption α_2 and refraction n_2 coefficient. Their values ($\alpha_2 = 7,2cm/GW$ and $n_2 = -3,9 \times 10^{-14}cm^2/GW$ can then be compared to the theoretical values. The theoretical value for the nonlinear absorption is derived similar to pertubation analysis following Cirloganu [40]

$$\alpha_2(\omega_1;\omega_2) = K\frac{\sqrt{E_p}}{n_1 n_2 E_{g^3}} F_2(\frac{\hbar\omega_1}{E_g};\frac{\hbar\omega_2}{E_g}) \tag{4.10}$$

with

$$F_2(x_1;x_2) = \frac{(x_1+x_2-1)^{\frac{3}{2}}}{2^7 x_1 x_2^2}(\frac{1}{x_1}+\frac{1}{x_2})^2 \tag{4.11}$$

and E_p as Kane energy parameter, E_g the band gap energy, K an independent material parameter and coupled to their respective wavelength, the refractive indizes n_1 and n_2 [41]. For the calculation of the nonlinear refraction index, one uses the Raman, Kerr and the quadratic Stark effect (QSE) to describe the nonlinear processes G_2.

$$n_2(\omega_1;\omega_2)\frac{\hbar cK}{2}\frac{\sqrt{E_p}}{n_1 n_2 E_g^4} G_2(\frac{\hbar\omega_1}{E_g};\frac{\hbar\omega_2}{E_g}) \tag{4.12}$$

While the nonlinear refraction coefficient (theoretical value $n_2 = -4,5 \times 10^{-14}cm^2/GW$) is still comparable, is the value for nonlinear absorption (theoretical value ($\alpha_2 = 11,7cm/GW$ with 40% difference pretty far of and so can our beam deflection experiment still not be considered as precise technique for the characterization of ZnO. A new fit program, handling large GVD could improve

that.

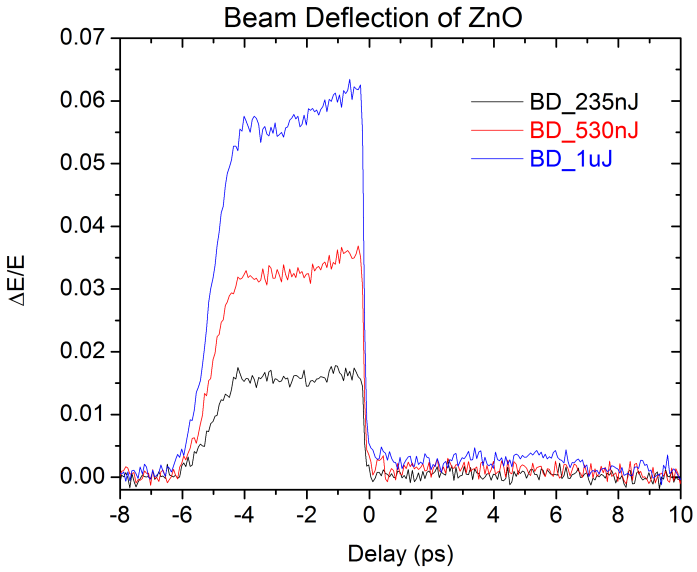

Figure 4.10: Beam deflection data of ZnO for three different excitation pulse energies $235nJ$(black), $530nJ$ (red) and $1000nJ$ (blue) $L = 0,53mm$, $\lambda_e = 800nm$, $\lambda_p = 400nm$, $w_e = 178\mu m$, $w_p = 45\mu m$, $\tau_e = 47fs$, $\tau_p = 100fs$

The determined negative sign of the nonlinear refractive index can be double-checked via a Z direction scan on the current beam deflection setup and compare it with the equivalent scan for fused silica. As the sign of the nonlinear refractive index of fused silica is known to be positive.

Noise reduction

One important concern in measuring small signals is always the noise, that reduces the accuracy of the measurement and the possible resolution. The present experiment already introduces plenty of noise reduction techniques, like the combination of chopper and lock-in amplifier (electronic) or the color filter and aperture in front of the detector (optic). To further improve the signal-noise

ratio a gaussian shape amplifier ($CrematCR - 200$) is tested. This amplifier accepts step input functions and translates them into amplified gaussian output functions. The idea is therefore to filter most of the noise from the signal. For the experiment the cross correlation in fused silica is performed with and without the gaussian shape amplifier, using the same experimental parameter (see figure 4.11).

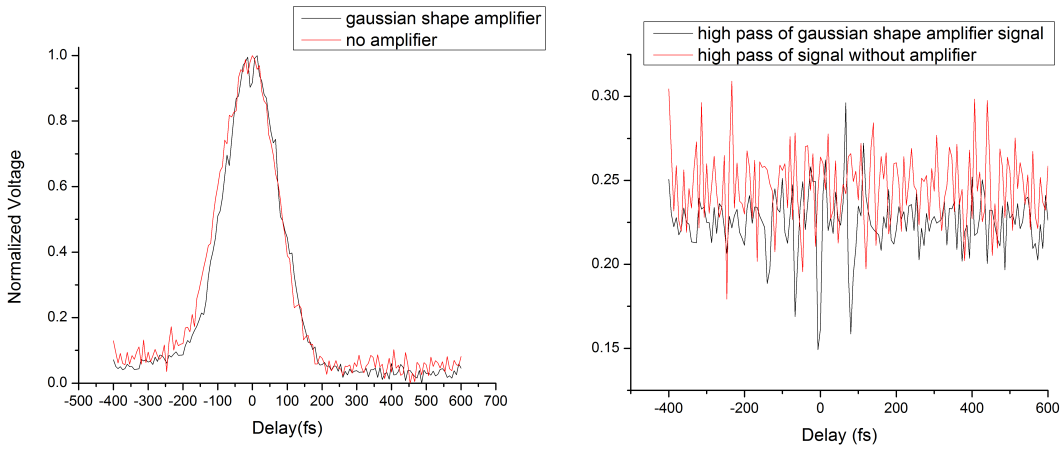

Figure 4.11: Normalized cross correlation in fused silica with and without gaussian shape amplifier (right) and noise compared after high pass filter (left)$L = 1mm$, $\lambda_e = 800nm$, $\lambda_p = 400nm$, $w_e = 178\mu m$, $w_p = 45\mu m$, $\tau_e = 47fs$, $\tau_p = 100fs$

Both normalized curves do not show big apparent differences as well as the noise levels are still very similar. Since the results did not promise any improvement on the experimental setup, the gaussian shape amplifier found no further use in this series of measurements.

CHAPTER 5: CONCLUSION

The aim of this work was to familiarize ourselves with some of the already established techniques to measure NLR and NLA of materials and examine a modification of the photothermal beam deflection as a new method of measurement to determine the nonlinear refractive index. These goals could be met for the most part. So were the results for the nonlinear refractive index of fused silica in good agreement with the literature and the difference between cross and co polarized measurement are according to the theory for isotropic material. Slight aberrations in particular for the comparison of the cross and co polarized measurements can still be explained with the noise level and therefore in acceptable limits. The time and polarization dynamic measurements for Carbon disulfide matches the provided theory to a high degree and can so be evaluated as good success for the effectiveness of the beam deflection measurement. Decomposing the nonlinear response into isotropic and reorientational response and comparing the result with the cross polarized measurement showed a good agreement. Also resolving NLR into fast and slow response was possible and the measured slow response was comparable with the literature value. Unfortunately was the used probe pulse duration too long to further resolve the fast response. The results from the first two samples left us with just two concerns, reducing the noise level and the pulse duration of the probe. As main reason for the long pulse duration of the probe, the narrow band pass filter after the WLC was identified. A series of experiments with different combinations of low and high pass filters were conducted to shorten the pulse. Even though the idea showed some promise with shorter pulses, the noise level increased drastically and made this effort mute. Another concern regarding the pulse length lies in the stability of the WLC and substituting the water cell with an BBO crystal for the ZnO measurement led as expected to a shortening of the pulse duration time. While the work on the probe pulse duration showed some improvement, the experiment to reduce the noise level was unsuccessful. Hereby a gaussian shape amplifier was tested and compared to the results

without. It turned out the noise levels of both measurements stayed about the same and no indication could be found to justify the use of the additional amplifier. The last experiment conducted throughout this work, was to determine the nonlinear properties of the wide gap semiconductor ZnO. Again this is done using our beam deflection technique and through a slight change of the experimental setup the pump probe technique. So the pump probe was used to determine the NLA of the sample and the NLR was measured with beam deflection. Both results are in the same order of magnitude as the calculated theoretical value, but in particular the measurement for the NLA is with 40% deviation not an overall satisfying result. Reason for the mismatch seemed to be the fitting process, that does not account for the large GVD. Although the quantitative results do not conform with the theoretical value in great accuracy, so can the nonlinear effects like GVM and GVD still be observed qualitatively. With little reservation can we count the work as success and the evaluated technique beam deflection as useful and accurate addition to the methods to determine nonlinear properties of material.

Future Work

There are different things to improve the setup and make it a more effective and variable apparatus. So could a optical parametric amplifier (OPA) be used to work with two variable wavelength for probe and excitation, the measurements could then be repeated with different wavelength combination. This could also enable a shorter probe pulse and the possibility to resolve the fast response of solvents like CS_2. Another advantage of the OPA could be a reduction of optical noise, since the generation of the probe pulse will be most likely improved compared to its generation with WLC and band pass filter. To further reduce the noise level, the current beam deflection setup will be new assembled to better shield the detectors from electronic noise sources.

LIST OF REFERENCES

[1] Sabra, A.I. (ed.): The Optics of Ibn al Haytham, 1983

[2] R.L.Verna: Al-Hazen: father of modern optic, 1969

[3] P. A. Franken, A. E. Hill, C. W. Peters, and G. Weinreich: Generation of Optical Harmonics, Phys. Rev. Lett. 7, 118 (1961)

[4] T. H. Maiman: Stimulated optical radiation in ruby, Nature, 187(4736):493-494, 1960

[5] Robert W. Boyd: Nonlinear Optics, New York: Academic Press, 3rd ed2008

[6] Jie Fu: Molecular structure nonlinear optical property relationships for a series of polymethine and squaraine molecules, University of Central Florida, 2006

[7] Ruzicka, B.A., et al.: Spatially resolved pump-probe study of single-layer graphene produced by chemical vapor deposition [Invited], Opt. Mater. Express, 2012. 2(6): p. 708-716

[8] Cho, G.C., W. Ktt, and H. Kurz: Subpicosecond time-resolved coherent-phonon oscillations in GaAs. Physical Review Letters, 1990. 65(6): p. 764-766

[9] Negres, R.A., et al.: Experiment and analysis of two-photon absorption spectroscopy using a white-light continuum probe, Quantum Electronics, IEEE Journal of, 2002. 38(9): p. 1205-1216

[10] Sheik-Bahae, M., et al.: Sensitive Measurement of Optical Nonlinearities Using a Single Beam, IEEE Journal of Quantum Electronics, 1990. 26(4): p. 10

[11] C. Spielmann: Lecture Grundlagen der Photonik, 2010

[12] H. Hu: Dissertation: Third Order Nonlinearity of organic molecules, University of Central Florida, 2012

[13] C. Cirloganu: Dissertation: Experimental and theoretical approaches to characterization of electronic nonlinearities in direct-gap semiconductors, University of Central Florida, 2010

[14] DeSalvo, R., et al.: Z-scan measurements of the anisotropy of nonlinear refraction and absorption in crystals, Opt. Lett., 1993. 18(3): p. 194-196

[15] Ma, H., A.S.L. Gomes, and C.B. de Araujo: Measurements of nondegenerate optical nonlinearity using a two-color single beam method, Applied Physics Letters, 1991. 59(21): p. 2666

[16] M. R. Ferdinandus et al.: Dual-arm Z-scan technique to extract dilute solute nonlinearities from solution measurements, Optical Material Express 1776, 2012, Vol.2, No. 12

[17] Boccara A. C., Fournier D. and Badoz J.: Thermo-optical spectroscopy: detection by the mirage effect, Appl. Phys. Lett. 36 1302,1980

[18] Bahaa E. A. Saleh, M. C. Teich: Fundamentals od Photonics (2nd Edition), Wiley, 2007

[19] L. W. Casperson: Gaussian light beams in inhomogeneous media, Applied Optics, Vol. 12, Issue 10, pp. 2434-2441 (1973)

[20] M. R. Ferdinandus et al.: Beam deflection measurement of time and polarization resolved ultrafast nonlinear refraction, University of Central Florida, 2013

[21] OSI Optoelectronics: Quadrant and Bi-Cell silicon photodiode amplifier module

[22] Stanford Research Systems: About lock-in amplifiers, application note 3

[23] COHERENT: Operator's manual Vitara modelocked Ti:S laser

[24] COHERENT: Operator's manual Coherent Legend Elite ultrafast amplifier laser systems

[25] D. Strickland, G. Mourou: Compression of amplified chirped optical pulses, Optics Communications,56(3):219-221, 1985

[26] J.-C. Diels, W. Rudolph: Ultrashort Laser Pulse Phenomena, Academic Press, 1996

[27] C. Fiorini, C. Sauteret, C. Rouyer, N. Blanchot, S. Seznec, and A. Migus: Temporal aberrations due to misalignments of a stretcher compressor system and compensation, Ieee Journal Of Quantum Electronics, 30(7):1662-1670, 1994

[28] COHERENT: Legend Elite Specification

[29] Guozhen Yang and Y. R. Shen: Spectral broadening of ultrashort pulses in a nonlinear medium, Optics Letters, Vol. 9, Issue 11, pp. 510-512 (1984)

[30] A. L. Gaeta: Catastrophic collapse of ultrashort pulses, Phys. Rev. Lett. 84, 35823585 (2000)

[31] R. R. Alfano and S. L. Shapiro: Observation of Self-Phase Modulation and Small-Scale Filaments in Crystals and Glasses, Phys. Rev. Lett. 24, Issue 11, pp. 592-594 (1970)

[32] R. A. Myers et al.: Large second-order nonlinearity in poled fused silica, Optics letters, Vol. 16, Issue 22, pp. 1732-1734 (1991)

[33] D. Milam, Appl. Opt. 37, 546-550 (1998)

[34] R. L. Sutherland. Handbook of Nonlinear Optics. Marcel Dekker Inc, New York, 2nd edition, 2003

[35] W. E. Williams, M. J. Soileau, and E. W. Van Stryland: Optical switching and n2 measurements in CS2. Optics Communications, 50(4):256 260, 1984

[36] W. Shensky III, I. Cohanoschi, F. E. Hernandez, E. W. Van Stryland, and D. J. Hagan:Broadband optical limiter using carbon-black suspensions in CS2. In Lasers and Electro-

Optics, 2002. CLEO 02. Technical Digest. Summaries of Papers Presented at the, page 572 vol.1, 2002

[37] Marcus Seidel: Thesis: Characterization of the nonlinear refractive index of Carbon Disulfide over an extended spectral and temporal range, University of Central Florida, 2011

[38] U. Ozgur, Ya.I. Alivov, C. Liu, A. Teke, M.A. Reshchikov, S. Dogan, V. Avrutin, S.-J. Cho, H. Morkoc,J. Appl. Phys., 98 (2005), p. 041301

[39] K. Kato: Second-Harmonic Generation to 2048A in Beta-Bariumborat; IEEE J. QE-22, 1013 (1986)

[40] Claudiu Cirloganu: Dissertation: Experimental and theoretical approaches to characterization of electronic nonlinearities in direct-gap semiconductors, University of Central Florida, 2010

[41] Kane E.O., "Band structure of indium antimonide". Journal of Physics and Chemistry of Solids, 1957. 1(4): p. 249-261

[42] Göppert-Mayer, M.: Über Elementarakte mit zwei Quantensprüngen, Ann. Phys (Leipzig), 9, 273-294, (1931)

[43] P. A.M. Dirac, Proc. ofR. S. vol. 114. S. 143 u. 710. 1927